

f-mode oscillations of compact stars in dynamical spacetimes: Equation of state dependencies and universal relations studies

Swarnim Shashank^{2,1}★ Fatemeh Hossein Nouri^{3,1}† Anshu Gupta¹‡

¹ Inter-University Centre for Astronomy and Astrophysics, Post Bag 4, Ganeshkhind, Pune 411 007, India

² Center for Field Theory and Particle Physics and Department of Physics, Fudan University, 200438 Shanghai, China.

³ Center for Theoretical Physics, Polish Academy of Sciences, Al. Lotnikow 32/46, 02-668 Warsaw, Poland

8 September 2021

ABSTRACT

In this article, we study the fundamental (*f*-)modes of non-rotating compact stars with realistic equations of state (EoS), extracted in the dynamical spacetime using numerical relativity simulations. We use a set of EoS with varying degree of stiffness and numerically evolve perturbed stellar models for several mass configurations (in the range of $1.2 - 2.0 M_{\odot}$) for each of these EoS. We observe the *f*-mode frequency is lower for the stiffer EoS, and it increases linearly with the square root of mean density for each set of EoS. We notice that the frequencies are distinguishable for soft, intermediate and stiffer EoS, thus it might be possible to constrain the EoS based on the detected signal frequency from the binary neutron star merger. More specifically for the softer EoS, the *f*-mode frequency is in the range of 1.8 – 2.2 kHz for the masses between $1.2 - 1.8 M_{\odot}$. On the other hand, in the case of stiffer EoS, such as 'BHB' and 'DD2' frequency is shifted to lower values 1.55 – 1.8 kHz for the same mass range. We also compare our single perturbed star simulation with recently studied binary simulations and find a good agreement.

Key words: stars: neutron – stars: oscillations – equation of state – methods: numerical

1 INTRODUCTION

Asteroseismology that enables us to understand the interior structure of neutron stars is coming to the forefront, with added tools of gravitational wave astronomy applied in detecting gravitational wave signal from two binary neutron star mergers (GW170817 Abbott et al. (2017) and GW190425 Abbott et al. (2020)), electromagnetic observations like NICER data; this assists in resolving degenerate parameters, puts stricter bounds on the internal composition of the star Miller et al. (2019); Bogdanov et al. (2019a,b); Raaijmakers et al. (2020); Jiang et al. (2020) and tests universal relations (UR).

Some of the parameters of neutron stars which could be inferred and estimated through multi-messenger astronomy are the mass, radius, spin, tidal deformability based on the mode frequencies extracted from the signals. While the joint mass, radius estimates using NICER data has put limits on the possible equations of state (EoS) which describes the internal composition Miller et al. (2019); Bogdanov et al. (2019a,b), incorporating tidal deformability information based on the GW170817 constraints further, the bounds on the permissible EoS Raaijmakers et al. (2020); Miller et al. (2020).

Some of the earlier works on gravitational asteroseismology includes Andersson & Kokkotas (1998); Allen et al. (1998); Pons et al. (2002); Benhar et al. (2004) (see Kokkotas (1996) for the pulsations of relativistic stars and references therein). Through multiple studies it has been shown that the fundamental oscillation mode (*f*-mode) of the star has a strong resonance with the orbital frequencies closer to merger of a coalescing binary neutron star. Resonant tidal excitation of oscillation modes in merging binary neutron stars has been carried out by Lai (1994); Lai & Wu (2006); Xu & Lai (2017). Other oscillation modes of the star, like p and g modes, may also become relevant throughout the inspiral, due to nonlinear coupling to the tide, as discussed by Weinberg et al. (2013); Weinberg (2016); Zhou & Zhang (2017); Nouri et al. (2021).

Schmidt & Hinderer (2019) describes an *f*-mode tidal model (fntidal) in the frequency domain under stationary phase approximation (SPA), discussed in Finn & Chernoff (1993). They compute tidal effects in the phase as described in Flanagan & Hinderer (2008). The Love numbers are measured by estimating the best-fit parameters using Poisson & Will (1995). Based on the "fntidal" model, Pratten et al. (2020) quotes *f*-mode frequency estimates using GW170817 data in the range of 1.37 – 1.47 and 1.47 – 1.59 kHz, (for the larger and the smaller NS mass companions, respectively) while taking into account the various PN order corrections and effects of adiabatic and dynamical tides. They also provide upper bounds by including the universal relations which are around

★ E-mail: sshashank20@fudan.edu.cn

† E-mail: f.h.noori@cft.edu.pl

‡ E-mail: anshu@iucaa.in

$\approx 2.8 - 2.9$ kHz and $\approx 3.1 - 3.2$ kHz for the two NS's. Phenomenological models connecting tidal deformability with frequency have been also discussed by [Andersson & Pnigouras \(2019, 2020\)](#).

Contribution due to spin during the binary neutron star merger on f -modes and dynamical tides have been recently carried out by [Ma et al. \(2020\)](#) and [Steinhoff et al. \(2021\)](#) based on some of the earlier works by [Hinderer et al. \(2010, 2016\)](#) and [Steinhoff et al. \(2016\)](#). Gravitational-wave asteroseismology with f -modes from neutron star binaries at the merger phase has been also carried out recently by [Ng et al. \(2020\)](#) where they use NR BNS simulations carried out in [Rezzolla & Takami \(2016\)](#); [Dietrich et al. \(2017a,b\)](#) and find less than one percent difference between BNS merger frequency (based on the merger peak amplitude) and f -modes computed for isolated neutron stars. They use the universal relations between f -mode and tidal deformability as given in [Chan et al. \(2014\)](#) to discuss UR between merger frequency and the rescaled tidal coupling parameter defined in terms of the dimensionless tidal Love numbers of the component neutron stars. Frequency deviations in the universal relations of isolated neutron stars and postmerger remnants have been discussed by [Lioutas et al. \(2021\)](#), whereas UR for damping time have been carried out in [Lioutas & Stergioulas \(2018\)](#).

Universal relations among compactness ($C = M/R$), moment of inertia (I) and tidal deformability, and their validity and deviations have been studied in [Maselli et al. \(2013\)](#); [Chan et al. \(2014\)](#); [Chirenti et al. \(2015\)](#); [Yagi & Yunes \(2017a\)](#) for the various choices of equations of state (see [Yagi & Yunes \(2017b\)](#) for review). [Jiang & Yagi \(2020\)](#) performs an analytical study showing about $\mathcal{O}(10^{-1})$ variation in the URs involving C (the compactness parameter) and I-Love relations having $\mathcal{O}(10^{-2})$ variations with numerical studies. They attribute it to the possible quadratic functionality of energy density as used in the Tolman VII solutions. Impact of the neutron-star deformability on equation of state parameters has been discussed by [Tsang et al. \(2020\)](#).

Series of studies have been performed in computing oscillation modes of neutron star using linear perturbation theory [Lindblom & Detweiler \(1983\)](#); [Detweiler & Lindblom \(1985\)](#); [Chirenti et al. \(2015\)](#). These studies are based on the standard approach laid out by [Thorne & Campolattaro \(1967\)](#) to solve the stellar perturbation equations in curved spacetime by applying the appropriate boundary conditions. The f -mode oscillations have also been studied using numerical simulations, employing the cowling approximation i.e. by evolving hydrodynamic equations in the fixed background of general relativistic spacetime for a single perturbed neutron star [Font et al. \(2000\)](#); [Font et al. \(2001\)](#); [Shibata & Karino \(2004\)](#); [Kastaun et al. \(2010\)](#); [Chirenti et al. \(2015\)](#), also in full GR to study bar mode instability [De Pietri et al. \(2014\)](#), as well as under conformally flatness condition (CFC) [Dimmelmeier et al. \(2006\)](#); [Bucciantini & Del Zanna \(2011\)](#); [Pili et al. \(2014\)](#) where the 3-metric is assumed to be conformally flat and the spacetime dynamics is coupled with fluid dynamics. [Ng et al. \(2020\)](#) employ CFC approach as discussed in [Dimmelmeier et al. \(2006\)](#) and use a publicly available code XNS described in [Bucciantini & Del Zanna \(2011\)](#); [Pili et al. \(2014\)](#).

Recently, [Rosofsky et al. \(2019\)](#) carried out studies in the fully dynamical spacetime and extracted the fundamental modes for the polytropic equations of state. There have been studies using piece-wise poly-tropic EoS to impose constraints on the neutron star structure [Bauswein et al. \(2020\)](#); [Miller et al. \(2020\)](#) or using the parametrised EoS with continuous sound speed [O'Boyle et al. \(2020\)](#). In the current work, we extract f -mode frequencies by evolving non-rotating neutron star in the dynamical spacetime while considering tabulated realistic EoS to describe its internal composition.

We also probe the possibility of using these single star simu-

lations to study the tidal effects expected during a binary inspiral by perturbing the stars in the Cowling regime and then evolving them using full General Relativity. Single star simulations are computationally less expensive to carry out, providing the possibility to reach higher resolutions in the future which may be important for studying higher order harmonics. We, further, study the validity of our results using the URs associated with tidal deformability and stellar parameters.

This is a step towards extending our study incorporating spin effects which we shall report in the follow up work. Our work provides leeway for future studies of tidal effects of rotating stars in an inspiral and also post-merger remnants with differential rotation.

In section 2 we briefly outline mathematical and numerical framework for general relativistic hydro-dynamical system, the initial setup and matter configuration as described by a set of equations of state under consideration. We analyse our simulation data and describe the result findings in section 3. We compute fundamental mode (f -mode frequency), its relations as a function of compactness and mass, then compare our fits with some of the recently carried out works. Our findings match well with the universal relations described with a deviation less than of a few percent. Section 4 discusses our results and conclusions. Appendix B briefly shows convergence test for our simulations.

2 BASIC NUMERICAL FRAMEWORK

We solve the Einstein equations using Numerical Relativity methods of 3+1 decomposition of the spacetime.

$$G_{\mu\nu} \equiv R_{\mu\nu} - \frac{1}{2}g_{\mu\nu}R = 8\pi T_{\mu\nu} \quad (1)$$

$$ds^2 = (-\alpha^2 + \beta_i\beta^i)dt^2 + 2\beta_i dx^i dt + \gamma_{ij} dx^i dx^j \quad (2)$$

[Alcubierre \(2008\)](#); [Rezzolla & Zanotti \(2013\)](#); [Baumgarte & Shapiro \(2010\)](#); [Shibata \(2015\)](#) here, α is the lapse function, β^i is the shift vector and γ_{ij} is the spatial metric.

The units used are $G = c = 1$ unless mentioned otherwise.

2.1 Dynamical evolution

The spacetime evolution is achieved using the Baumgarte-Shapiro-Shibata-Nakamura-Oohara-Kojima (BSSNOK) formalism ([Nakamura et al. 1987](#); [Shibata & Nakamura 1995](#); [Baumgarte & Shapiro 1998](#); [Alcubierre et al. 2000](#)) which is a conformal formulation of the ADM equations ([Arnowitt et al. 1959, 2008](#)). The (1+log) and Gamma-driver gauge conditions are adopted for the evolution of lapse and shift ([Alcubierre 2008](#); [Baiotti & Rezzolla 2017](#)). We use the MACLACHLAN code ([Brown et al. 2009](#)) for evolution of spacetime variables which is a publicly available code in the EINSTEINTOOLKIT ([Babiuc-Hamilton et al. 2019](#); [Goodale et al. 2003](#); [Schnetter et al. 2006, 2004](#)) suite. A Kreiss-Oliger dissipation ([Rezzolla & Zanotti 2013](#); [Alcubierre 2008](#); [Shibata 2015](#)) is added to spacetime variables for removing high frequency noise.

To model Neutron stars, a relativistic perfect fluid is assumed. The conservation equations for the energy-momentum tensor $T_{\mu\nu}$ and the matter current density J_μ , are solved numerically after being recast into a flux-conservative formulation ([Rezzolla & Zanotti 2013](#); [Font 2008](#); [Baiotti & Rezzolla 2017](#))

$$\nabla_\mu J^\mu = 0, \nabla_\mu T^{\mu\nu} = 0 \quad (3)$$

The system of equations is complete with an Equation of State

of the type $p = p(\rho, Y_e, T)$ which for our models is described in the sec. 2.3. (For more details readers can refer to (Rezzolla & Zanotti 2013; Font 2008; Baiotti & Rezzolla 2017; Shibata 2015).)

We carry out the hydrodynamics using the publicly available WhiskyTHC code (Radice et al. 2013, 2014; Radice, D. & Rezzolla, L. 2012) which works within the EINSTEINTOOLKIT framework and uses high-resolution shock capturing methods. For the time integration, method of lines is used with fourth-order Runge-Kutta methods. The fifth-order MP5 flux-reconstruction method is used along with Harten-Lax-van Leer-Einfeldt (HLLE) Riemann solver.

2.2 Initial data

We use a perturbed Tolman–Oppenheimer–Volkoff (TOV) star for the initial data. The initial data is generated using the PizzaTOV thorn for both polytropic and tabulated equations of state. A perturbation is added for the density as:

$$\delta\rho = \mathcal{A}\rho(r/R)Y_{22} \quad (4)$$

where, $\delta\rho$ is the perturbed density, ρ is the density, \mathcal{A} is the perturbation amplitude which we set to 0.01 to introduce a small perturbation, r is the radial distance from centre of the star and R is the radius of the star. We use the (2,2) eigenfunction which is expected to be similar to tidal interactions of binary neutron stars (Rosofsky et al. 2019; Pratten et al. 2020). For all the models we choose the artificial background atmosphere density as $\rho_{atm} = 10^{-14} M \approx 6.17 \times 10^3 g cm^{-3}$.

The simulations are performed at minimum grid spacing of $0.105M \approx 155m$. For the tabulated EoS $1.4M_\odot$ cases we also perform simulations at $0.07M$ and for polytrope at $0.06M$. The convergence test for the DD2 equation of state for three different resolutions is given in appendix B.

2.3 Equations of State

We use several finite-temperature, composition dependent nuclear-theory based equations of state (fig. 1). Three of them are based on relativistic mean field (RMF) models. These equations of state are publicly available in tabulated form at <https://stellarcollapse.org>.

(i) LS220 Lattimer & Swesty (1991) (Lattimer & Swesty EoS with the incompressibility $K = 220$ MeV): contains neutrons, protons, alpha particles and heavy nuclei. It is based on the single nucleus approximation for heavy nuclei. LS220 has been widely used in many supernova simulations.

(ii) DD2 Hempel et al. (2012): contains neutrons, protons, light nuclei such as deuterons, helions, tritons and alpha particles and heavy nuclei. DD2 is an RMF with a density-dependent nucleon-meson coupling for treating high density nuclear matter.

(iii) SFHo Steiner et al. (2013): Another RMF, and similar to DD2 it contains neutrons, protons, light nuclei such as deuterons, helions, tritons and alpha particles and heavy nuclei. However, the RMF parameters are tuned to fit the NS mass-radius observation.

(iv) BHB Banik et al. (2014): Another RMF similar to DD2 and SFHo with the same particle composition, but BHB EoS additionally includes Λ hyperons and hyperon-hyperon interactions allowed by ϕ mesons.

(v) SLy Chabanat et al. (1998): contains only protons, neutrons and electrons. It is developed out of a refined Skyrme-like effective potential, originating from the shell-model description of the nuclei.

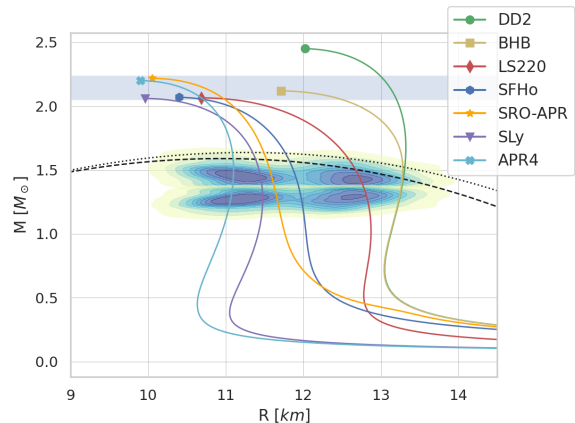


Figure 1. A comparison of all the equation of states used. The dotted line represents our polytropic model with $\kappa = 100$ and the dashed line represents the polytropic model $\kappa = 94.29$ (see Eq. 5). The shaded region is the range of observed mass of pulsar *J0740 + 6620* (Cromartie et al. 2020). Purple-Blue region in the middle is the parametrised EoS $M - R$ relation obtained from *GW170817* (Abbott et al. 2018).

(vi) APR4: is the complete version of a four-realistic-EoS series developed by Akmal, Pandharipande and Ravenhall Akmal et al. (1998), named APR1 through 4, obtained from potentials resulting from fits to nucleon-nucleon scattering. APR4 includes the relativistic corrections and the three nucleon interaction potential additionally, which makes it more complete in comparison with the other APRs. This EoS is commonly used in neutron star simulations, as it occurs to be compatible with astronomical observations.

(vii) SRO-APR Schneider et al. (2019): is based on APR potential model. However, similar to Lattimer & Swesty EoS, it assumes compressible liquid droplet model of nuclei. It contains neutrons, protons, a single type of heavy nucleus plus alpha particles representing light nuclei.

For testing our methods, we also use a polytropic equation of state model

$$p = \kappa\rho^\Gamma \quad (5)$$

We use $\Gamma = 2$ and choosing accordingly the values of κ and central density, we create models for stars of masses $1.35M_\odot$ and $1.4M_\odot$. We evolve this model as well as the SLy and APR4 models using a hybrid equation of state approach (Takami et al. 2015; Figura et al. 2020) viz. a gamma-law correction for finite temperature with $\Gamma_{th} = 2$. The evolution equation of state becomes:

$$P(\rho, \epsilon) = P_{cold}(\rho) + \rho[\epsilon - \epsilon_{cold}(\rho)](\Gamma_{th} - 1) \quad (6)$$

We find that the results obtained from the hybrid equation of state method for our $1.4M_\odot$ polytrope to be consistent with the results from ref. (Rosofsky et al. 2019).

3 ANALYSIS AND RESULTS

We evolve a set of non-rotating configurations in the mass range of $1.2 - 2.0M_\odot$ for each of the EoS, described in section 2.3. The mass, radius, central density for these have been listed in the first four columns of table 2. The frequency of the mode is computed by taking the Fourier transform of the time series data for the gravitational waveform generated during the evolution of each simulation. For

EoS	a	b
DD2	0.657	32.061
BHB	0.429	39.801
LS220	0.286	44.653
SFHo	0.663	35.101
SRO-APR	0.881	29.958
SLy	0.557	36.544
APR4	0.795	30.791

Table 1. Data fitted for the various compact star models with Eq. 7. We find that our results are in agreement with the ref. (Chirenti et al. 2015).

smoothing the peaks in the FFTs we use cubic spline. We consider the waveform that is extracted at the radius $r = 10M$ for the $l = 2$, $m = 2$ mode of the Ψ_4 data using the Newman-Penrose formalism (Newman & Penrose 1963; Bishop & Rezzolla 2016). We choose this radius since it has the least amount of noise among all the considered extraction radii while the computed fundamental mode stays the same as could be seen in Fig. B4.

We also notice that change in resolution does not affect the extracted f -mode frequencies Fig. B3 (appendix B). We run the simulations for $2100M \approx 10.35ms$.

3.1 fundamental (f)-modes

We present our models and results of our simulations in table 2. In Fig. 2 (top panels) we plot the f -mode frequency value in terms of mass and compactness for the considered set of equations of state.

We notice that the f -mode frequency is much smaller for the stiff EoS such as DD2 and BHB. It increases for the higher masses and softer EoS. Based on the frequency band of the observed gravitational signal and the inferred mass, it is possible to put bounds on the soft/stiffness of the EoS that characterises the interior of the neutron star. For example, if the detected f -mode frequency is below 1.8 kHz for a star having mass above $1.4M_\odot$, then all the considered soft EoS would be ruled out. On the other hand, frequency above 1.8 kHz would permit only some stiff EoS if the object is more massive i.e. $\approx 1.8M_\odot$ or more and compactness above 0.20. Similar trends we see in terms of effective compactness η and tidal deformability λ_2 (see bottom panels of Fig. 2). We also observe that while few of the considered EoS show linear trend, some of the other, such as BHB, LS220, SLy and SFHo deviate and show a faster rise in f -mode values for larger parameter values (as could be seen in all the four panels of Fig 2). This doesn't seem to be dependent only on the softness or stiffness of the matter, but could be due to the finer micro-physics involved. To understand this better, in our follow-up studies, we plan to consider a larger set of EoS, including the ones having hyperons, strange quark matter, etc.

In Fig. 3 we present the fits of our models with the relation as given in ref. (Chirenti et al. 2015) :

$$f = a + b \sqrt{\frac{M}{R^3}} \quad (7)$$

We find a good linear fit for our data across the EoS used for our study and list the values of a and b in table 1. LS220 EoS shows the steepest change (the red line), followed by BHB (the Beige color line) in Fig. 3. We compare our fit obtained in table 1 to the Table II in ref. (Chirenti et al. 2015) for the LS220 and APR4 equation of states, and find our results to be in agreement (within 10%).

3.2 Universal Relations

In order to study, whether the equations of state specific trends that we notice above, contribute to the deviation from Universal relations or not, we verify some of the URs. First, we compute the relation between f -mode frequency and the tidal deformability as given in (Pratten et al. 2020; Chan et al. 2014)

$$M\omega = \sum_i a_i (\xi)^i \quad (8)$$

where a_i are the numerical coefficients presented in table 3. M is the mass of the star and ω is the angular f -mode frequency. $\xi = \log(\lambda_2)$ where λ_2 is the dimensionless electric tidal deformability calculated from the tidal Love number k_2 as (Chan et al. 2014):

$$\lambda_2 = \frac{2}{3} \frac{k_2}{(M/R)^5} \quad (9)$$

The tidal Love number k_2 is calculated by solving the metric perturbation equation as defined in ref. (Hinderer 2008). For this computation we integrate Eq. (15) from Hinderer (2008) for the metric perturbation function H , from center to surface using fourth order Runge-Kutta method. We use the Runge-Kutta ODE solver with adaptive step size routine from Numerical recipe Press et al. (2007). Finally, the tidal Love number k_2 is computed from Eq.(23) from Hinderer (2008). Figure 2 (bottom-right panel) shows the relation of tidal deformability λ_2 with the f -mode.

The comparison and deviation for f -Love UR, Eq. 8 is carried out in two ways: first, using these equations we compute the coefficients for our data. Second, using the same values of coefficients as given in ref. (Chan et al. 2014) but, with the f , λ_2 and η that we calculate for each of our simulation. The last three columns of table 2 show comparison and percent deviations with f -Love UR's. Table 3 lists the coefficients for ref. (Chan et al. 2014) and the ones computed for our data. In fig. 4 we compare the our results with that of ref. (Chan et al. 2014).

It has been observed that universal behaviour also exist between the f -mode and the effective compactness η (Lau et al. 2010; Chirenti et al. 2015). We also test these URs described by the model

$$M\omega = c_1 + c_2 \eta + c_3 \eta^2 \quad (10)$$

where $\eta = \sqrt{M^3/I}$ and I is the moment of inertia. We obtain the fit as $c_1 = -0.00747$, $c_2 = 0.1471$ and $c_3 = 0.55328$. We show this universality in the fig. 5. Our results agree well with the results of the earlier works (Lau et al. 2010; Chirenti et al. 2015). The fundamental mode f -mode and effective compactness η that we compute for our configurations are also plotted in Fig 2 (bottom left panel).

Universal relation between the compactness and tidal Love numbers have been discussed in appendix A.

3.3 Calculation of damping times

We compute fundamental frequency from Ψ_4 data of our simulations (see discussion in the beginning of section 3) by evolving each initial configuration for about $2100M$ (≈ 10 ms). This duration is insufficient, and it is required to have a longer simulation and higher resolution to extract reliable damping times. Thus, we choose the recently established relations, which use compactness and effective

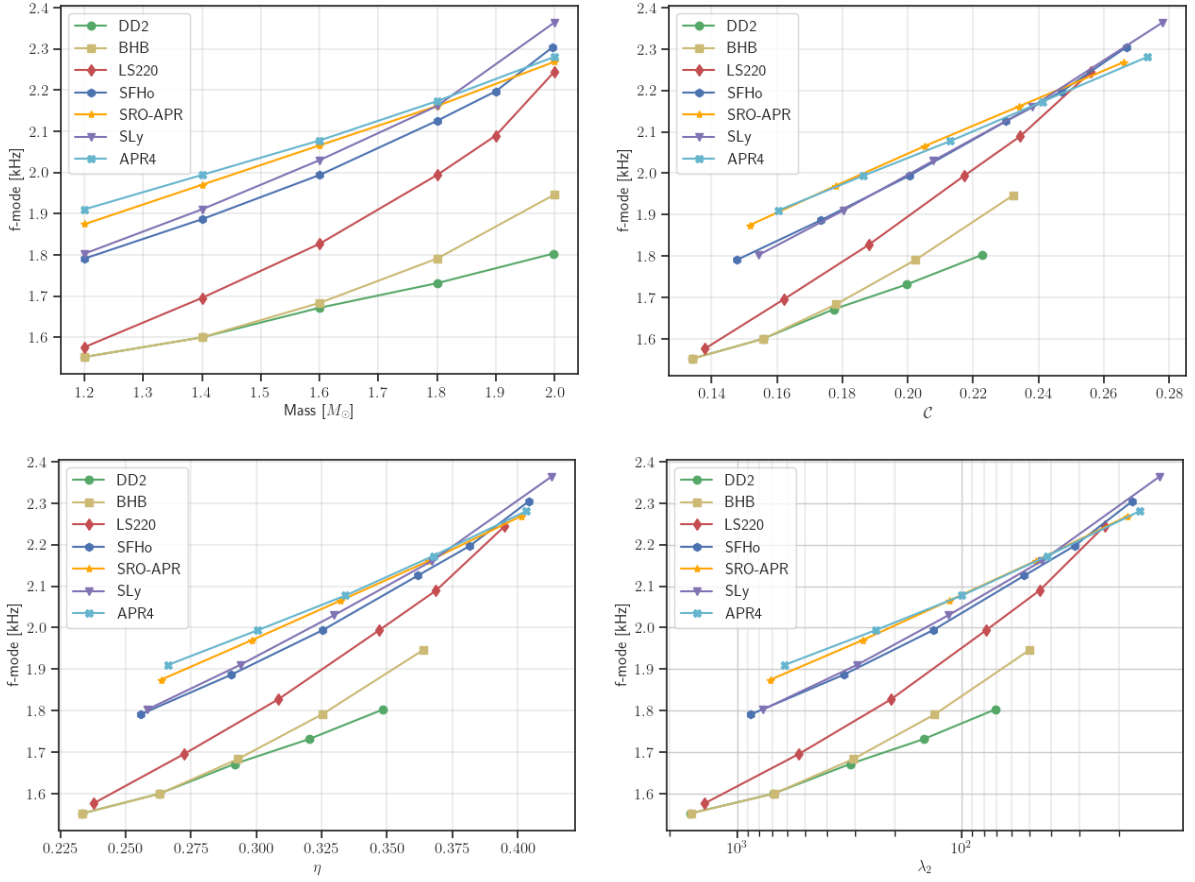


Figure 2. *f*-mode frequency for different EoS is shown in different panels with respect to mass M (top left); compactness $C = M/R$, R being the radius of the star (top right); effective compactness $\eta = \sqrt{M^3/I}$ where I is the moment of inertia (bottom left) and tidal deformability λ_2 as in Eq. 9 (bottom right). The softer EoS has larger *f*-mode frequencies as compared to the intermediate (LS220) and stiffer (DD2 and BHB) EoS.

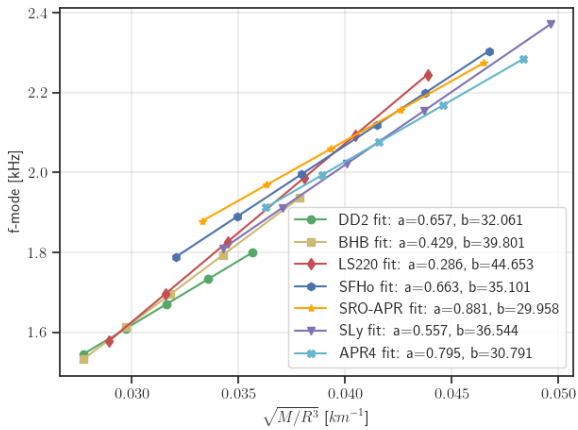


Figure 3. Fit from Eq.7. The a and b values are listed on the figure above and also table 1.

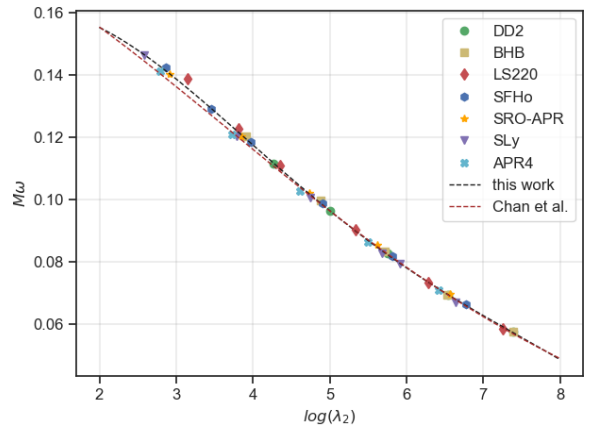


Figure 4. The universality observed between tidal deformability and *f*-modes. Here, we compare our fit with that of ref. (Chan et al. 2014).

compactness for calculating the damping times (Lioutas & Stergioulas 2018; Chirenti et al. 2015):

$$\frac{M}{\tau_1} = 0.112 \left(\frac{M}{R}\right)^4 - 0.53 \left(\frac{M}{R}\right)^5 + 0.628 \left(\frac{M}{R}\right)^6 \quad (11)$$

$$\frac{I^2}{M^5 \tau_2} = 0.0068 - 0.025 \eta^2 \quad (12)$$

where τ_1 and τ_2 are the damping times in terms of compactness $C = \frac{M}{R}$ and effective compactness η , respectively. Figure 6 shows

EoS	Mass (M_{\odot})	Radius (km)	Central Density (g/cm^3)	f -mode (kHz)	k2	UR difference (%) (Chan et al. 2014)	UR difference (%) (This work)	(%)-difference (Chan et al. 2014) v. This work
Polytrope	1.35	13.80	8.22×10^{14}	1.6237	0.0805	1.99	2.21	0.22
	1.4	14.15	7.91×10^{14}	1.5730	0.0793	0.77	1.03	0.26
DD2	1.2	13.20	5.25×10^{14}	1.5522	0.1061	0.46	0.71	0.25
	1.4	13.27	5.73×10^{14}	1.5998	0.0953	0.57	0.24	0.33
	1.6	13.31	6.27×10^{14}	1.6715	0.0833	0.02	0.55	0.53
	1.8	13.30	6.9×10^{14}	1.7312	0.0709	0.05	0.00	0.05
	2.0	13.24	7.67×10^{14}	1.8028	0.0586	0.55	0.31	0.86
BHB	1.2	13.20	5.25×10^{14}	1.5521	0.1058	0.35	0.59	0.24
	1.4	13.27	5.84×10^{14}	1.5998	0.0947	0.72	0.38	0.34
	1.6	13.26	6.73×10^{14}	1.6834	0.0821	0.05	0.57	0.53
	1.8	13.13	8.0×10^{14}	1.7909	0.0675	1.11	1.04	0.08
	2.0	12.71	1.02×10^{15}	1.9461	0.0508	2.17	0.87	1.29
LS220	1.2	12.84	6.16×10^{14}	1.5760	0.1056	1.34	1.20	0.14
	1.4	12.75	7.19×10^{14}	1.6954	0.0898	0.57	0.11	0.46
	1.6	12.56	8.47×10^{14}	1.8267	0.0734	0.27	0.62	0.35
	1.8	12.23	1.03×10^{15}	1.9936	0.0568	1.92	1.18	0.74
	1.9	11.96	1.16×10^{15}	2.0893	0.0482	2.42	1.00	1.41
	2.0	11.53	1.37×10^{15}	2.2446	0.0383	4.15	2.30	1.80
SFHo	1.2	11.99	7.41×10^{14}	1.7909	0.0922	0.48	0.69	0.21
	1.4	11.92	8.4×10^{14}	1.8864	0.0793	0.17	0.72	0.54
	1.6	11.79	9.6×10^{14}	1.9938	0.0653	0.41	0.35	0.06
	1.8	11.56	1.12×10^{15}	2.1252	0.0511	1.37	0.13	1.23
	1.9	11.36	1.24×10^{15}	2.1968	0.0436	1.57	0.14	1.71
	2.0	11.05	1.43×10^{15}	2.3042	0.0355	2.40	0.68	1.72
SRO-APR	1.2	11.68	8.03×10^{14}	1.8744	0.0862	0.54	0.86	0.32
	1.4	11.61	8.9×10^{14}	1.9699	0.0745	0.38	0.88	0.50
	1.6	11.51	9.87×10^{14}	2.0655	0.0620	0.63	0.37	0.26
	1.8	11.35	1.11×10^{15}	2.1610	0.0495	0.99	0.37	1.37
	2.0	11.09	1.27×10^{15}	2.2684	0.0368	1.68	0.06	1.75
SLy	1.2	11.47	7.79×10^{14}	1.8028	0.1016	1.67	1.39	0.28
	1.35	11.46	8.58×10^{14}	1.8983	0.0885	0.77	0.23	0.55
	1.4	11.46	8.86×10^{14}	1.9103	0.0840	1.48	0.97	0.52
	1.6	11.37	1.02×10^{15}	2.0296	0.0670	0.85	1.09	0.24
	1.8	11.16	1.2×10^{15}	2.1610	0.0506	0.08	1.49	1.43
	2.0	10.62	1.55×10^{15}	2.3639	0.0328	1.21	0.20	1.41
APR4	1.2	11.04	8.24×10^{14}	1.9103	0.0984	0.89	0.49	0.40
	1.4	11.09	9.12×10^{14}	1.9938	0.0818	1.15	0.71	0.44
	1.6	11.09	1.01×10^{15}	2.0774	0.0661	1.17	1.57	0.41
	1.8	11.01	1.14×10^{15}	2.1729	0.0512	0.46	1.92	1.49
	2.0	10.81	1.32×10^{15}	2.2804	0.0371	0.44	1.19	1.66

Table 2. f -modes for the different EoS for different masses. A clear trend is visible. Frequency increases with mass and with softness of the EoS. Agreement of f -Love URs (Chan et al. 2014; Pratten et al. 2020) is also presented for the different models for $l = 2$ by calculating the %-difference between LHS and RHS of Eq.8. Second to last two columns are obtained by fitting the UR with our data. And the last column lists the difference between the UR provided in (Chan et al. 2014) and our work.

Fit	a_0	a_1	a_2	a_3	a_4
(Chan et al. 2014)	1.820×10^{-1}	-6.836×10^{-3}	-4.196×10^{-3}	5.215×10^{-4}	-1.857×10^{-5}
This work	1.442×10^{-1}	3.005×10^{-2}	-1.607×10^{-2}	2.092×10^{-3}	-9.247×10^{-5}

Table 3. Fitting parameters a_i from Eq.8 for the f -Love universal relations. Comparing this work and (Chan et al. 2014). The a_i values have been calculated without the polytropic models.

damping time vs frequency plot, where the damping time is taken to be the average of τ_1 and τ_2 . We find that for the polytrope case one of the relations overestimates the damping time obtained from linear perturbations methods (Baiotti et al. 2009; Rosofsky et al. 2019) while the other underestimates, taking an average of τ_1 and τ_2 gives us a value close to the expected value for the polytrope, hence we report the average values. In the subsequent study, we intend to extract damping times by evolving our systems for a much

longer time and at a much higher resolution as one needs to be sure that the damping obtained is not due to numerical errors.

4 CONCLUSIONS

In this work, we evolve isolated non-spinning Neutron star in fully dynamical spacetime. We consider a set of realistic EoS as listed in section 2.3 to describe internal composition of the star. For each of the considered EoS, we evolve 5-6 configurations having mass in

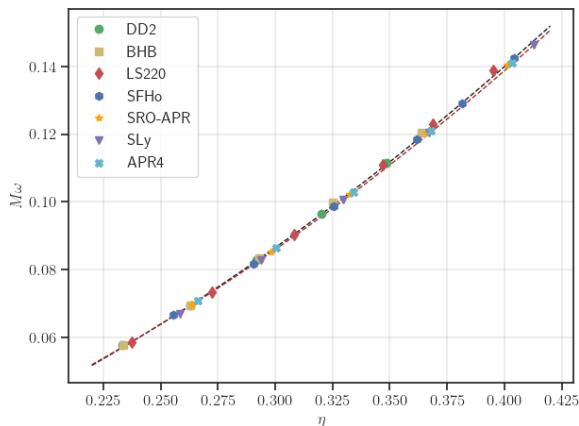


Figure 5. The universality observed between η and f -mode. The black dashed line is the fit that we obtained for Eq. 10. The brown dashed line is the one presented in the ref. (Chirenti et al. 2015).

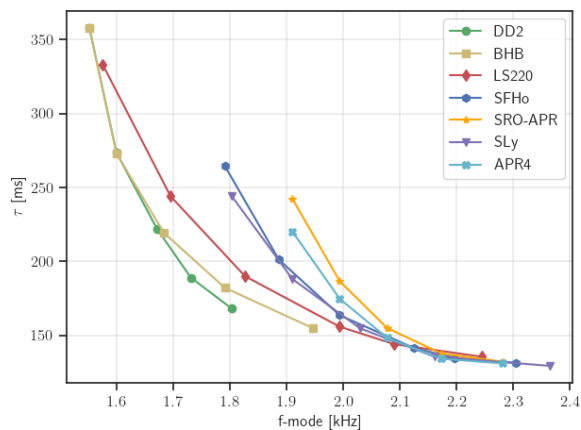


Figure 6. f -mode vs the damping time for all the models. The damping time here is calculated as $(\tau_1 + \tau_2)/2$ from Eq. 11 and Eq. 12.

the range of $1.2 - 2.0M_{\odot}$. We compute f -mode frequency for each of the case and its dependence on the equation of state. We also compute tidal deformability for each of the case using perturbative approach.

Our analysis show evidence of approximate universal relations between f -mode and other neutron star parameters such as tidal deformability, compactness etc, as have been reported in the past. However, there is still a possibility to distinguish and constrain the possible stiff or soft equations of state based on the observed gravitational wave signal, as f -mode frequency value differs almost by 0.5 kHz for soft EoS (APR4) and stiff EoS (DD2 or BHB) when the mass of the neutron star is $1.4M_{\odot}$. The difference is higher for the more massive cases, in fact, for $M \geq 1.8M_{\odot}$, frequency differs by ≈ 300 Hz between DD2 (stiff EoS) and LS220 (having intermediate stiffness). Frequency computed are also well within the bounds reported by ref. (Pratten et al. 2020) through Bayesian estimates.

Further, the computed frequencies match very well with the studies performed by other groups while studying the fundamental modes during the binary neutron star merger as well as the frequencies extracted through perturbative studies. In particular, we simulated couple of configuration to compare the f -mode frequency

with ref. (Steinhoff et al. 2021), where they extract the f -mode frequency using numerical relativity simulation of binary systems. We obtain an excellent match with their results, comparing to their black hole - neutron star binary simulation using $1.35M_{\odot}$ polytrope, we find a deviation of 0.6% and with their neutron star - neutron star binary simulation using $1.35M_{\odot}$ SLy EoS we see a deviation of only 0.03%. We further note that even by interpolating the mass vs f -mode data based on our simulations to get the f -mode frequency at $1.35M_{\odot}$, the value which we get differs only by 0.9% for the SLy EoS from the one reported in ref. Steinhoff et al. (2021).

These findings indicate that using single perturbed star simulations could give us similar results to that of a binary simulation, saving on computational time and resources. We also observe, similar tidal behaviour for SRO-APR and APR4 EoS, where the former is one of the most updated EoS in the family of APR EoS, hence it could be a good choice for binary merger simulations for future studies.

Our f -mode study of a perturbed neutron star in this paper is limited in many ways. We considered only non-rotating stars, and our EoS selection includes only one EoS with exotic matter i.e. BHB with hyperons. In the follow-up studies, it is important to perform dynamical spacetime simulations of a perturbed rotating neutron star to investigate the relativistic corrections on f -mode frequency shift due to spin effects Steinhoff et al. (2021). Further, these studies can be enhanced by including a broad range of EoS with hyperons Pradhan & Chatterjee (2021), strange or hybrid matter, and also considering the parametrized EoS with piece-wise polytropic EoS Bauswein et al. (2020); Miller et al. (2020) or with continuous sound speed O’Boyle et al. (2020) to impose constraints on EoS, as are being considered in some of the recent studies. In addition, we intend to consider longer evolution with higher resolution to have a better accuracy for the higher mode measurements, as well as for the f -mode damping time measurements.

ACKNOWLEDGMENTS

The authors thank Sukanta Bose for frequent helpful discussions, scientific advice and comments over the entire course of this project. We thank D. Radice for help and support with WhiskyTHC code. We are also grateful to Sukanta Bose and P. Pnigouras for carefully proof reading the manuscript and giving useful inputs. S.S. acknowledges L. Baiotti, I. Hawke and International Centre for Theoretical Sciences (ICTS) for discussions during the program - Gravitational Wave Astrophysics (Code: ICTS/Prog-gws2020/05). Part of this research is supported by the Navajbai Ratan Tata Trust and LIGO-India funds at IUCAA, India. F.H. acknowledges grant No. 2019/35/B/ST9/04000 from the Polish National Science Center, Poland. S.S. also acknowledges support from the China Scholarship Council (CSC), Grant No. 2020GXZ016646. The numerical simulations for this work were performed on Pegasus cluster, which is a part of the high performance computing (HPC) facility at The Inter-University Centre for Astronomy and Astrophysics (IUCAA), Pune, India.

DATA AVAILABILITY

The data underlying this article will be shared on reasonable request to the corresponding authors.

REFERENCES

- Abbott B. P., et al., 2017, *Phys. Rev. Lett.*, 119, 161101
- Abbott B. P., et al., 2018, *Phys. Rev. Lett.*, 121, 161101
- Abbott B. P., et al., 2020, *The Astrophysical Journal*, 892, L3
- Akmal A., Pandharipande V. R., Ravenhall D. G., 1998, *Phys. Rev. C*, 58, 1804
- Alcubierre M., 2008, *Introduction to 3+1 Numerical Relativity*. Oxford University Press, Oxford
- Alcubierre M., Brügmann B., Dramlitsch T., Font J. A., Papadopoulos P., Seidel E., Stergioulas N., Takahashi R., 2000, *Phys. Rev. D*, 62, 044034
- Allen G., Andersson N., Kokkotas K. D., Schutz B. F., 1998, *Phys. Rev. D*, 58, 124012
- Andersson N., Kokkotas K. D., 1998, *Monthly Notices of the Royal Astronomical Society*, 299, 1059
- Andersson N., Pnigouras P., 2019, The phenomenology of dynamical neutron star tides ([arXiv:1905.00012](https://arxiv.org/abs/1905.00012))
- Andersson N., Pnigouras P., 2020, *Phys. Rev. D*, 101, 083001
- Arnowitt R., Deser S., Misner C. W., 1959, *Phys. Rev.*, 116, 1322
- Arnowitt R., Deser S., Misner C. W., 2008, *General Relativity and Gravitation*, 40, 1997
- Babiuc-Hamilton M., et al., 2019, The Einstein Toolkit, [doi:10.5281/zenodo.3522086](https://doi.org/10.5281/zenodo.3522086)
- Baiotti L., Rezzolla L., 2017, *Reports on Progress in Physics*, 80, 096901
- Baiotti L., Bernuzzi S., Corvino G., De Pietri R., Nagar A., 2009, *Phys. Rev. D*, 79, 024002
- Banik S., Hempel M., Bandyopadhyay D., 2014, *The Astrophysical Journal Supplement Series*, 214, 22
- Baumgarte T. W., Shapiro S. L., 1998, *Phys. Rev. D*, 59, 024007
- Baumgarte T., Shapiro S., 2010, *Numerical Relativity: Solving Einstein's Equations on the Computer*. Cambridge University Press
- Bauswein A., et al., 2020, *Phys. Rev. Lett.*, 125, 141103
- Benhar O., Ferrari V., Gualtieri L., 2004, *Phys. Rev. D*, 70, 124015
- Bishop N. T., Rezzolla L., 2016, *Living Reviews in Relativity*, 19, 2
- Bogdanov S., et al., 2019a, *ApJ*, 887, L25
- Bogdanov S., et al., 2019b, *ApJ*, 887, L26
- Brown D., Diener P., Sarbach O., Schnetter E., Tiglio M., 2009, *Phys. Rev. D*, 79, 044023
- Bucciantini N., Del Zanna L., 2011, *A&A*, 528, A101
- Chabananat E., Bonche P., Haensel P., Meyer J., Schaeffer R., 1998, *Nucl. Phys. A*, 635, 231
- Chan T. K., Sham Y.-H., Leung P. T., Lin L.-M., 2014, *Phys. Rev. D*, 90, 124023
- Chirenti C., de Souza G. H., Kastaun W., 2015, *Phys. Rev. D*, 91, 044034
- Cromartie H. T., et al., 2020, *Nature Astronomy*, 4, 72
- De Pietri R., Feo A., Franci L., Löffler F., 2014, *Phys. Rev. D*, 90, 024034
- Detweiler S., Lindblom L., 1985, *ApJ*, 292, 12
- Dietrich T., Ujevic M., Tichy W., Bernuzzi S., Brügmann B., 2017a, *Phys. Rev. D*, 95, 024029
- Dietrich T., Bernuzzi S., Ujevic M., Tichy W., 2017b, *Phys. Rev. D*, 95, 044045
- Dimmelmeier H., Stergioulas N., Font J. A., 2006, *Monthly Notices of the Royal Astronomical Society*, 368, 1609
- Figura A., Lu J.-J., Burgio G. F., Li Z.-H., Schulze H.-J., 2020, *Phys. Rev. D*, 102, 043006
- Finn L. S., Chernoff D. F., 1993, *Phys. Rev. D*, 47, 2198
- Flanagan E. E., Hinderer T., 2008, *Phys. Rev. D*, 77, 021502
- Font J. A., 2008, *Living Reviews in Relativity*, 11, 7
- Font J. A., Stergioulas N., Kokkotas K. D., 2000, *Mon. Not. Roy. Astron. Soc.*, 313, 678
- Font J. A., Dimmelmeier H., Gupta A., Stergioulas N., 2001, *Monthly Notices of the Royal Astronomical Society*, 325, 1463
- Godzieba D. A., Gamba R., Radice D., Bernuzzi S., 2021, *Phys. Rev. D*, 103, 063036
- Goodale T., Allen G., Lanfermann G., Massó J., Radke T., Seidel E., Shalf J., 2003, in *Vector and Parallel Processing – VECPAR'2002*, 5th International Conference, Lecture Notes in Computer Science. Springer, Berlin, <http://edoc.mpg.de/3341>
- Hempel M., Fischer T., Schaffner-Bielich J., Liebendörfer M., 2012, *The Astrophysical Journal*, 748, 70
- Hinderer T., 2008, *The Astrophysical Journal*, 677, 1216–1220
- Hinderer T., Lackey B. D., Lang R. N., Read J. S., 2010, *Phys. Rev. D*, 81, 123016
- Hinderer T., et al., 2016, *Phys. Rev. Lett.*, 116, 181101
- Jiang N., Yagi K., 2020, *Phys. Rev. D*, 101, 124006
- Jiang J.-L., Tang S.-P., Wang Y.-Z., Fan Y.-Z., Wei D.-M., 2020, *ApJ*, 892, 55
- Kastaun W., Willburger B., Kokkotas K. D., 2010, *Phys. Rev. D*, 82, 104036
- Kokkotas K. D., 1996, Pulsating relativistic stars, <http://arxiv.org/abs/gr-qc/9603024>
- Lai D., 1994, *MNRAS*, 270, 611
- Lai D., Wu Y., 2006, *Phys. Rev. D*, 74, 024007
- Lattimer J. M., Swesty F. D., 1991, *Nucl. Phys.*, A535, 331
- Lau H. K., Leung P. T., Lin L. M., 2010, *ApJ*, 714, 1234
- Lindblom L., Detweiler S. L., 1983, *Astrophys. J. Suppl.*, 53, 73
- Lioutas G., Stergioulas N., 2018, *Gen Relativ Gravit*, 50
- Lioutas G., Bauswein A., Stergioulas N., 2021, *Phys. Rev. D*, 104, 043011
- Ma S., Yu H., Chen Y., 2020, *Phys. Rev. D*, 101, 123020
- Maselli A., Cardoso V., Ferrari V., Gualtieri L., Pani P., 2013, *Phys. Rev. D*, 88, 023007
- Miller M. C., et al., 2019, *ApJ*, 887, L24
- Miller M. C., Chirenti C., Lamb F. K., 2020, *ApJ*, 888, 12
- Mösta P., et al., 2013, *Classical and Quantum Gravity*, 31, 015005
- Nakamura T., Oohara K., Kojima Y., 1987, *Progress of Theoretical Physics Supplement*, 90, 1
- Newman E., Penrose R., 1963, *Journal of Mathematical Physics*, 4, 998
- Ng H. H.-Y., Cheong P. C.-K., Lin L.-M., Li T. G. F., 2020, Gravitational-wave asteroseismology with f-modes from neutron star binaries at the merger phase ([arXiv:2012.08263](https://arxiv.org/abs/2012.08263))
- Nouri F. H., Bose S., Duez M. D., Das A., 2021, arXiv e-prints, [p. arXiv:2107.13339](https://arxiv.org/abs/2107.13339)
- O'Boyle M. F., Markakis C., Stergioulas N., Read J. S., 2020, *Phys. Rev. D*, 102, 083027
- Pili A. G., Bucciantini N., Del Zanna L., 2014, *Monthly Notices of the Royal Astronomical Society*, 439, 3541
- Poisson E., Will C. M., 1995, *Phys. Rev. D*, 52, 848
- Pons J. A., Berti E., Gualtieri L., Miniutti G., Ferrari V., 2002, *Phys. Rev. D*, 65, 104021
- Pradhan B. K., Chatterjee D., 2021, *Phys. Rev. C*, 103, 035810
- Pratten G., Schmidt P., Hinderer T., 2020, *Nature Communications*, 11, 2553
- Press W. H., Teukolsky S. A., Vetterling W. T., Flannery B. P., 2007, *Numerical Recipes 3rd Edition: The Art of Scientific Computing*. Cambridge University Press
- Raaijmakers G., et al., 2020, *ApJ*, 893, L21
- Radice D., Rezzolla L., 2012, *A&A*, 547, A26
- Radice D., Rezzolla L., Galeazzi F., 2013, *Monthly Notices of the Royal Astronomical Society: Letters*, 437, L46
- Radice D., Rezzolla L., Galeazzi F., 2014, *Classical and Quantum Gravity*, 31, 075012
- Rezzolla L., Takami K., 2016, *Phys. Rev. D*, 93, 124051
- Rezzolla L., Zanotti O., 2013, *Relativistic Hydrodynamics*. Oxford University Press, Oxford
- Rosofsky S. G., Gold R., Chirenti C., Huerta E. A., Miller M. C., 2019, *Phys. Rev. D*, 99, 084024
- Schmidt P., Hinderer T., 2019, *Phys. Rev. D*, 100, 021501
- Schneider A. S., Constantinou C., Muccioli B., Prakash M., 2019, *Phys. Rev. C*, 100, 025803
- Schnetter E., Hawley S. H., Hawke I., 2004, *Classical and Quantum Gravity*, 21, 1465
- Schnetter E., Diener P., Dorband E. N., Tiglio M., 2006, *Classical and Quantum Gravity*, 23, S553
- Shibata M., 2015, *Numerical Relativity*. World Scientific Publishing Company
- Shibata M., Karino S., 2004, *Phys. Rev. D*, 70, 084022
- Shibata M., Nakamura T., 1995, *Phys. Rev. D*, 52, 5428
- Sotani H., 2021, *Phys. Rev. D*, 103, 123015

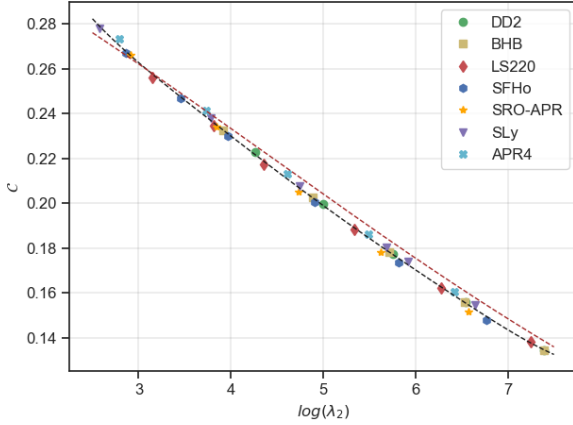


Figure A1. The universality observed between tidal deformability and compactness. Here, we compare our fit (black dashed line) with that of ref. (Godzieba et al. 2021) (brown dashed line).

Steiner A. W., Hempel M., Fischer T., 2013, *The Astrophysical Journal*, 774, 17
 Steinhoff J., Hinderer T., Buonanno A., Taracchini A., 2016, *Phys. Rev. D*, 94, 104028
 Steinhoff J., Hinderer T., Dietrich T., Foucart F., 2021, *Phys. Rev. Research*, 3, 033129
 Stergioulas N., Friedman J. L., 1995, *Astrophysical Journal*, 444, 306
 Takami K., Rezzolla L., Baiotti L., 2015, *Physical Review D*, 91, 064001
 Thorne K. S., Campolattaro A., 1967, *ApJ*, 149, 591
 Tsang C. Y., Tsang M. B., Danielewicz P., Lynch W. G., Fattoyev F. J., 2020, *Phys. Rev. C*, 102, 045808
 Weinberg N. N., 2016, *The Astrophysical Journal*, 819, 109
 Weinberg N. N., Arras P., Burkart J., 2013, *The Astrophysical Journal*, 769, 121
 Xu W., Lai D., 2017, *Phys. Rev. D*, 96, 083005
 Yagi K., Yunes N., 2017a, *Class. Quant. Grav.*, 34, 015006
 Yagi K., Yunes N., 2017b, *Phys. Rept.*, 681, 1
 Zhou Y., Zhang F., 2017, *The Astrophysical Journal*, 849, 114

APPENDIX A: COMPACTNESS - TIDAL DEFORMABILITY UNIVERSAL RELATIONS

For our compact star models, we also study another universal relation in addition to the discussion in sec.3.2 between the compactness and tidal Love number using the initial data that we use in our simulations. We also use this as a check for our initial data against already established results (Maselli et al. 2013; Godzieba et al. 2021). The universal relations are given as,

$$C = \sum_i b_i (\log(\lambda_2))^i \quad (\text{A1})$$

The universal relation between compactness and tidal deformability provides us the constraint on the radius of the star as a less compact star will be deformed more by a tidal potential for a given mass (Godzieba et al. 2021), providing a relation between radius and λ_2 . We present our obtained fit for b_i in table A1. In fig. A1, we compare our results to a recent study by (Godzieba et al. 2021). Our results are consistent with the results of (Maselli et al. 2013).

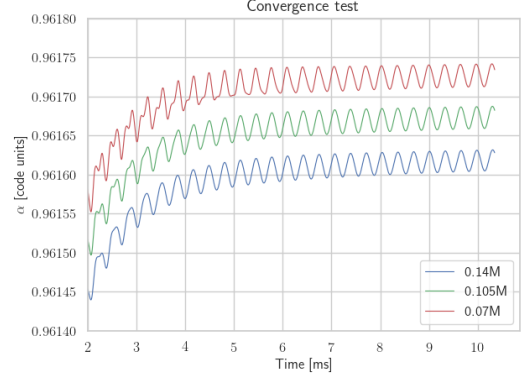


Figure B1. The central lapse for three different resolutions. Convergence can be seen.

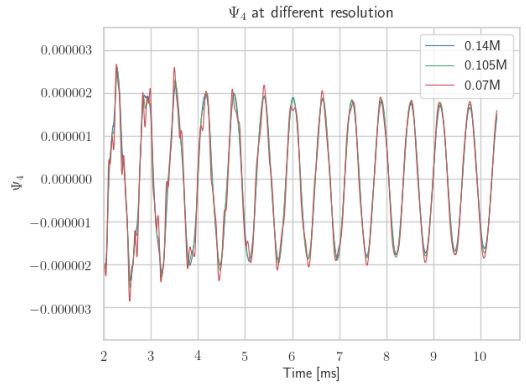


Figure B2. Ψ_4 plotted at three different resolution. The change in resolution does not change the Ψ_4 data.

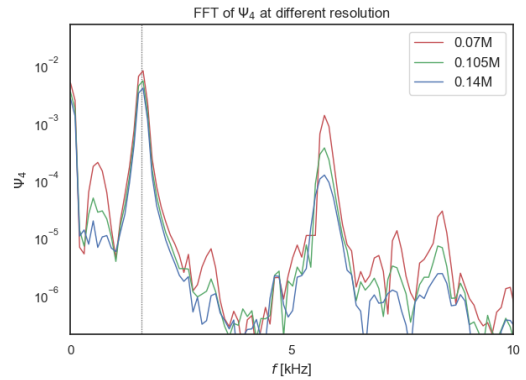


Figure B3. The FFT of Ψ_4 at three different resolution shows the *f*-mode value does not change. The black dashed line represents the value of *f*-mode frequency.

APPENDIX B: NUMERICAL TESTS

B1 *f*-mode frequency at different resolutions

The performance of `whiskyTHC` code has been tested before Radice et al. (2013). Here we only test the accuracy of our results within the selected resolution for our simulations. In order to claim that the resolution is in the convergence regime, we perform a multiple

Fit	b_0	b_1	b_2	b_3	b_4	b_5	b_6
(Maselli et al. 2013)	3.71×10^{-1}	-3.91×10^{-2}	1.056×10^{-3}				
This work	3.770×10^{-1}	-4.137×10^{-2}	1.149×10^{-3}				
(Godzieba et al. 2021)	3.388×10^{-1}	-2.30×10^{-2}	-4.651×10^{-4}	-2.636×10^{-4}	5.424×10^{-5}	-3.188×10^{-6}	6.181×10^{-8}
This work	7.951×10^{-1}	-5.839×10^{-1}	2.877×10^{-1}	-7.908×10^{-2}	1.205×10^{-2}	-9.628×10^{-4}	3.155×10^{-5}

Table A1. Fitting parameters b_i from Eq.A1 for the C -Love universal relations. Comparing this work with the coefficient values in (Maselli et al. 2013) and (Godzieba et al. 2021). The values of b_i 's have been calculated without using the polytrope EoS cases.

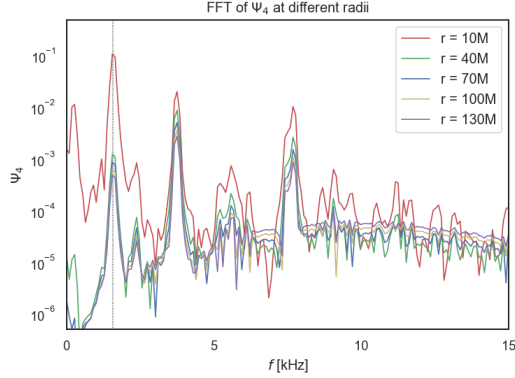


Figure B4. The FFT of Ψ_4 at 5 different radii with a refinement layer between each.

resolutions test for a single case, i.e. DD2 EoS with $M = 1.4M_\odot$. We choose our standard resolution with grid spacing equals to $0.105M$ as the intermediate level, and $0.07M$ and $0.14M$ as the higher and lower resolutions respectively.

The results of this test are presented in Fig. B1 for the lapse function, and Fig. B2 for Ψ_4 function. The Fourier transform over Ψ_4 , which gives the oscillation frequency spectrum is shown in Fig B3. These results indicate that the observed quantities converge to one solution as we move from low to high resolutions, and the value of f -mode frequencies do not change significantly across different resolutions. This convergence study confirms that the intermediate resolution used in our numerical simulations, to report the f -mode frequencies, is in the convergence regime.

B2 f -mode frequency at different Ψ_4 extraction radii

As the second numerical test, we investigate the accuracy of the Ψ_4 functions extracted from different radii. For this test we choose our polytropic case with $\Gamma = 2$, $\kappa = 100$ and $M = 1.4M_\odot$, with minimum grid spacing equals to $0.06M$ for the resolution. The Ψ_4 outputs are extracted at $r = 10, 40, 70, 100, 130M$ for the Fourier transform.

In fig. B4, we show that the f -mode frequency does not change with different radii of extraction of Ψ_4 for Polytropic equation of state. We also notice that f -mode is most prominent and has less noise for $r = 10M$, and hence we chose it for comparison in with other equations of state.

This paper has been typeset from a $\text{\TeX}/\text{\LaTeX}$ file prepared by the author.